WARWICK
THE UNIVERSITY OF WARWICK

Manuscript version: Author's Accepted Manuscript
The version presented in WRAP is the author's accepted manuscript and may differ from the published version or Version of Record.

Persistent WRAP URL:
http://wrap.warwick.ac.uk/135294

How to cite:
Please refer to published version for the most recent bibliographic citation information. If a published version is known of, the repository item page linked to above, will contain details on accessing it.

Copyright and reuse:
The Warwick Research Archive Portal (WRAP) makes this work by researchers of the University of Warwick available open access under the following conditions.

© 2020 Elsevier. Licensed under the Creative Commons Attribution-NonCommercial-NoDerivatives 4.0 International http://creativecommons.org/licenses/by-nc-nd/4.0/.

Publisher's statement:
Please refer to the repository item page, publisher's statement section, for further information.

For more information, please contact the WRAP Team at: wrap@warwick.ac.uk.

warwick.ac.uk/lib-publications

Journal Pre-proof

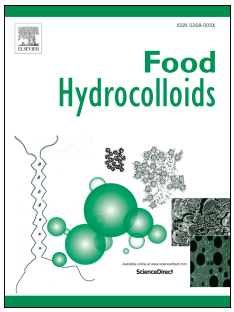

Understanding the structure and rheological properties of potato starch induced by hot-extrusion 3D printing

Zipeng Liu, Huan Chen, Bo Zheng, Fengwei Xie, Ling Chen

PII: S0268-005X(19)32993-5

DOI: https://doi.org/10.1016/j.foodhyd.2020.105812

Reference: FOOHYD 105812

To appear in: *Food Hydrocolloids*

Received Date: 23 December 2019

Revised Date: 19 February 2020

Accepted Date: 25 February 2020

Please cite this article as: Liu, Z., Chen, H., Zheng, B., Xie, F., Chen, L., Understanding the structure and rheological properties of potato starch induced by hot-extrusion 3D printing, *Food Hydrocolloids* (2020), doi: https://doi.org/10.1016/j.foodhyd.2020.105812.

This is a PDF file of an article that has undergone enhancements after acceptance, such as the addition of a cover page and metadata, and formatting for readability, but it is not yet the definitive version of record. This version will undergo additional copyediting, typesetting and review before it is published in its final form, but we are providing this version to give early visibility of the article. Please note that, during the production process, errors may be discovered which could affect the content, and all legal disclaimers that apply to the journal pertain.

© 2020 Published by Elsevier Ltd.

Journal Pre-proof

CRediT author statement:

Zipeng Liu: Methodology, Validation, Formal analysis, Investigation, Data Curation, Writing - Original Draft, Visualization. **Huan Chen:** Methodology, Validation, Formal analysis, Investigation. **Bo Zheng:** Methodology, Investigation, Writing - Review & Editing. **Fengwei Xie:** Conceptualization, Methodology, Resources, Writing - Review & Editing, Visualization, Supervision, Funding acquisition. **Ling Chen:** Conceptualization, Methodology, Resources, Supervision, Project administration, Funding acquisition.

Journal Pre-proof

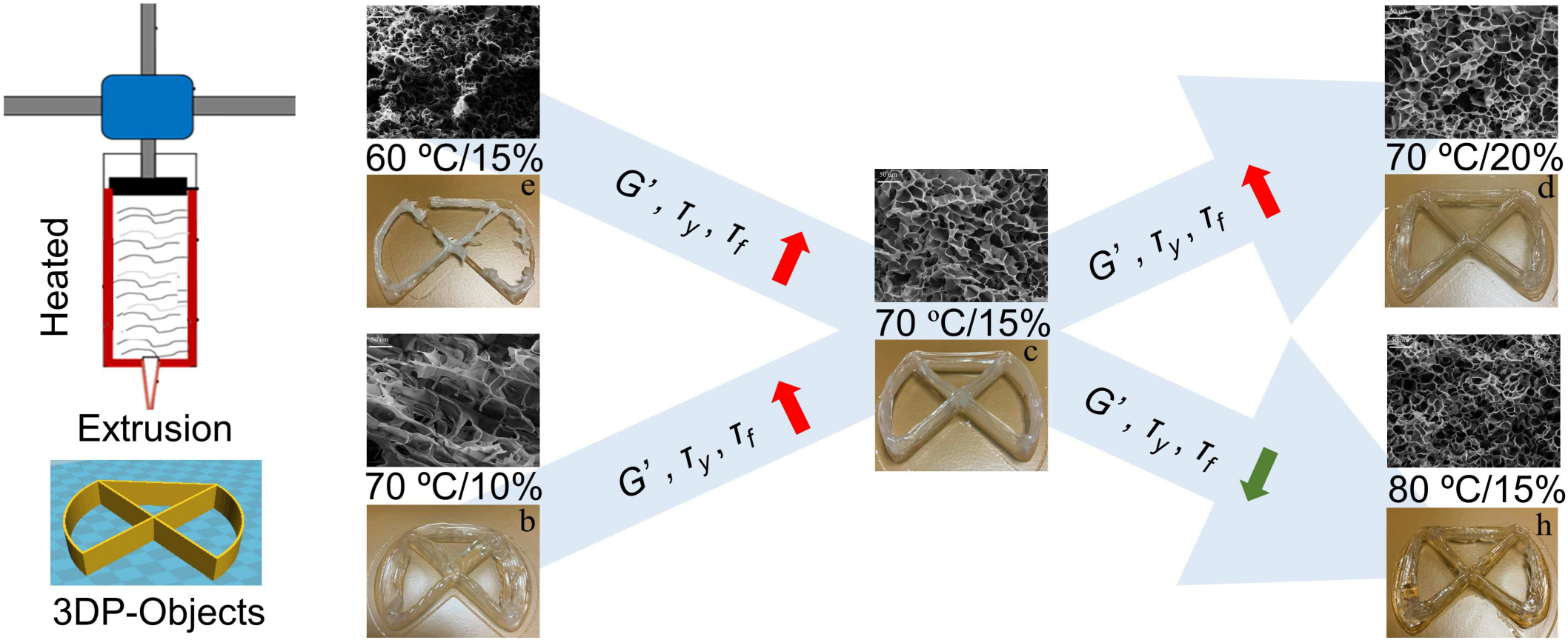
Heated
Extrusion
3DP-Objects
60 ºC/15%
e
70 ºC/10%
b
G', Ty, Tf
G', Ty, Tf
70 ºC/15%
c
G', Ty, Tf
G', Ty, Tf
70 ºC/20%
d
80 ºC/15%
h

Journal Pre-proof

Understanding the structure and rheological properties of potato starch induced by hot-extrusion 3D printing

Zipeng Liu [a], Huan Chen [a], Bo Zheng [a], Fengwei Xie [b,c,**], Ling Chen [a,*]

[a] *Ministry of Education Engineering Research Center of Starch & Protein Processing, Guangdong Province Key Laboratory for Green Processing of Natural Products and Product Safety, School of Food Science and Engineering, South China University of Technology, Guangzhou 510640, China*

[b] *International Institute for Nanocomposites Manufacturing (IINM), WMG, University of Warwick, Coventry CV4 7AL, United Kingdom*

[c] *School of Chemical Engineering, The University of Queensland, Brisbane, Qld 4072, Australia*

**Corresponding author. Email: felchen@scut.edu.cn (L. Chen)

* Corresponding Author. Email: d.xie.2@warwick.ac.uk; f.xie@uq.edu.au (F. Xie)

Abbreviations

HE-3DP, hot-extrusion 3D printing; PS, potato starch; τ_f, flow stress; τ_y, yield stress; G', storage modulus; LVR, linear viscoelastic region

Journal Pre-proof

Journal Pre-proof

Abstract: This work investigates the 3D printability of potato starch (PS). For this purpose, the structure and rheological properties of the PS-based ink under hot-extrusion 3D printing (HE-3DP) at different PS concentrations and printing temperatures were studied. PS concentration was found to determine the structure and rheological properties of the PS gel. The printing temperature was shown to influence the structural transformation of PS and closely linked to the rheological properties of the gel. PS samples of 15–25% concentration at 70 °C presented optimal printability, which showed the absence of the original granule, crystalline and lamellar structures, with the formation of a uniform and compact gel network. In this case, the rheological properties were in a suitable range for HE-3DP including G' (615.72–1057.63 Pa), τ_y (89.389–263.25 Pa) and τ_f (490.00–1104.97 Pa), which provided the PS-based ink with smooth extrusion, excellent printing accuracy and high structural strength, suitable for applications such as food and biomedical materials.

Keywords: Potato starch; Hot-extrusion 3D printing; Structure; Rheological properties; Printability

Journal Pre-proof

Journal Pre-proof

1 Introduction

With the development of food processing, food 3D printing has become an innovative and disruptive food technology as it provides unique potential advantages such as customized designs and simple operation (Dankar, Haddarah, Omar, Sepulcre, & Pujolà, 2018). Food 3D printing has changed the concept of traditional food preparation, which is well received by customers (Sun, Zhou, Yan, Huang, & Lin, 2018). During 3D printing, food is constructed by layer-by-layer deposition according to a pre-designed model; moreover, the food quality and nutrition can be improved through the rational selection of raw materials (Liu, Zhang, & Yang, 2018c; Yang, Zhang, Bhandari, & Liu, 2018; Dong et al., 2019). Nowadays, hot extrusion and binder jetting are most commonly used among all food 3D printing techniques. In particular, hot-extrusion 3D printing (HE-3DP) has drawn much attention due to its high printing accuracy and ability to handle a wide range of food sources (Sun, Zhou, Huang, Fuh, & Hong, 2015). Based on the research of food 3D printing, all soft food materials can be used for HE-3DP, while the rheological properties of food materials are crucial for the printability, including extrudability and supportability. Food materials should have appropriate flow stress and mechanical strength to ensure smooth extrusion from the nozzle and the sufficient support to the next printed layer without deformation or collapse (Godoi , Prakash, & Bhandari, 2016; Le Tohic et al., 2018; Yang, Zhang, Fang, & Liu, 2019).

Potato starch (PS) has been widely used in the food industry due to its unique nutritional value and processing properties, and its production scale and product development have been growing quickly (Ibanoğlu , Özaslan, & Ibanoğlu, 2018). Due to the high degree of polymerization, PS shows the characteristics of easy expansion and high viscosity (Han et al., 2019). When PS is

Journal Pre-proof

used as a HE-3DP material to produce personalized PS-based food, its rheological properties may be a key factor to affect its printability (Ai & Jane, 2015; Przetaczek-Rożnowska, 2017). PS paste is a kind of pseudoplastic fluid with shear-thinning behavior, thus can be extruded easily under high-shear printing (Zhang, Li, Zhang, Wei, & Fang, 2019b). After extrusion, the molecular chains rearrange rapidly to form a gel network structure by hydrogen bonding and chain entanglement, which endows printed objects with mechanical strength (Zheng et al., 2019). Yang et al. (2018) showed that PS could adjust the rheological properties of lemon juice gels for a new 3D printed food. Liu, Zhang, Bhandari, and Yang (2018b) indicated that 2% (w/w) PS mashed potato had optimal flow behavior during extrusion as reflected by consistency index and flow behavior index. They also found that in the printed material, there was a distinct layered structure in the longitudinal section while a porous structure in the transverse section (Liu, Bhandari, Prakash, & Zhang, 2018a). Lille, Nurmela, Nordlund, Metsä-Kortelainen, and Sozer (2018) suggested that the shape stability of printed objects was positively correlated with the yield stress of the printed materials (Lille et al., 2018).

PS concentration and printing temperature can be two of the key factors in controlling the printability during the HE-3DP process (Dankar, Pujolà, El Omar, Sepulcre, & Haddarah, 2018). A high PS concentration means a greater number of starch chains in the system, which increases the chance of hydrogen bonding and chain entanglement, thus increasing the viscosity and storage modulus of the starch paste (Guo, Hu, Zhang, & Du, 2016). A high temperature facilitates the destruction of intermolecular hydrogen bonds in the starch granule and makes the resulting starch paste presenting low yield stress and high loss tangent. Subsequent cooling leads the starch paste to

form a stable network structure and provide it with mechanical strength (Krystyjan, Ciesielski, Khachatryan, Sikora, & Tomasik, 2015). A higher temperature has also been found to decrease the consistency coefficient and yield stress of PS paste (Martínez-Monzó, Cárdenas, & García-Segovia, 2019). Chen, Xie, Chen, and Zheng (2019) concluded that starch pastes with concentrations of 15–25% at 70–85 °C possessed preferable flow stress and yield stress, thus excellent printability, for HE-3DP.

Despite the advantages of HE-3DP, the research on 3D printing of starch-based products has just been started. Moreover, while most of the studies focused on the rheological properties and printability of starch-based materials, the correlation among the structure, rheological properties and printability have much rarely been attempted. These relationships, however, are crucial for the design of personalized high-quality starch-based food by HE-3DP. In the study, we investigated the changes in the structure and rheological properties of PS paste during HE-3DP at different concentrations and printing temperatures, which are correlated with the printability of the paste.

2 Material and methods

2.1 Materials

Potato starch (PS) was provided by Qinuo Food Ingredients Co., Ltd. (Zhengzhou, China), which contains 15.54% moisture and 34.5% amylose. Double distilled water was used in this work.

2.2 Sample preparation

PS suspensions were prepared according to our reported method (Chen et al., 2019). A PS suspension of 3% (w/w, dry basis) concentration was heated and stirred at 65 °C for 20 min. After

cooling to room temperature, more PS was added into the suspension to achieve different concentrations (10, 15, 20, 25 and 30%, w/w, dry basis).

HE-3DP was performed on a SHINNOVE-S2 printer (Shiyin, China). First, the prepared PS suspension was poured into the feed cylinder, heated to the printing temperature (60, 65, 70, 75 or 80 °C) and equilibrated for 5 min. Then, printing was carried out based on a premade model and the printed objects were photographed to record the line width and layer number (Liu, Zhang, Bhandari, & Wang, 2017). The printing parameters included a nozzle height of 1.0 mm, a nozzle diameter of 0.8 mm, a nozzle speed of 30 mm/s, a pulling rate of 50 mm/s, and a pulling distance of 2 mm.

2.3 Scanning electron microscopy (SEM)

Printed objects were cryo-fractured and then freeze-dried. The samples were sputter-coated with gold and then examined using an EM-30 Plus scanning electron microscope (COXEM, Korea) operated at 20 kV with 500× magnification (Cieśla, Sartowska, & Królak, 2015).

2.4 X-ray diffraction (XRD)

The freeze-dried samples were pulverized and sieved through 0.15 mm and equilibrated at a fixed relative humidity (75%, achieved using saturated NaCl) for 24 h before the XRD analysis. The crystalline structure and relative crystallinity of starches were analyzed with an Xpert PRO diffractometer (Panalytical, Netherlands), following our published method (40 mA, 50 kV, Cu-Kα radiation) (Liu, Chen, Xu, Liang, & Zheng, 2019).

2.5 Attenuated total reflectance-Fourier transform Infrared spectroscopy (ATR-FTIR)

FTIR spectroscopy for freeze-dried samples was performed using a Nicolet iS50 instrument

(Thermo Fisher Scientific, USA) with an attenuated total reflectance (ATR) accessory, following our previous method (Liu et al., 2019)

2.6 Small-angle X-ray scattering (SAXS)

SAXS measurements were performed on a SAXSess system (Anton-Paar, Austria) according to our previous method (50 mA, 40 kV, Cu Kα radiation) (Chi et al., 2017). The samples were measured instantly after printing.

The SAXS spectra of starch samples were fitted by the Ornstein-Zernike (OZ) equation (Emmerling et al., 1995; Hammouda, Ho, & Kline, 2004; Juszczak, Witczak, Ziêba, & Fortuna, 2012):

$$I(q) = \frac{Ioz\,(0)}{1+\xi^2 q^2} \qquad \text{(Eq.1)}$$

where $I(q)$ is the scattering intensity, q is the scattering vector, and ξ is the correlation length of starch samples.

2.7 Rheological measurements

Rheological properties were performed on an MCR302 rheometer (Anton Paar, Austria) with a parallel-plate geometry (25 mm diameter and 1 mm gap). Printed samples in the original gel state were loaded and equilibrated at the test temperature for 5 min. Then, the exposed edge of the sample was covered with a thin layer of silicone oil to prevent moisture evaporation. Strain sweep tests in a range of 0.001–10 at 1 Hz in the oscillation mode were performed (Chen, Zhang, Li, Xie, & Chen, 2018). The data were analyzed using RheoCompass 1.21 software to obtain storage modulus (G'), yield stress (τ_y), and flow stress (τ_f). τ_y is defined as the point in the linear-viscoelastic range where G' decreased by 3%; τ_f is identified as the cross point of the G' and G'' curves ($G' = G''$)

(Mirarab Razi, Motamedzadegan, Shahidi, & Rashidinejad, 2018).

2.8 Statistical analysis

All tests were conducted at least in triplicate and the experimental data were analyzed using SPSS statistics 23.0 (IBM, Armonk, NY, USA). One-way analysis of variance was used to find the significant difference by Duncan's test ($p < 0.05$). The correlation was evaluated by Pearson correlation analysis.

3 Results and discussion

3.1 Morphology

Fig. 1 shows the morphology of 3D-printed PS samples under different HE-3DP conditions. PS samples at different concentrations all formed a spongy network structure but with different degrees of cell density. This indicates that under the HE-3DP conditions, PS underwent sufficient gelatinization and the interaction between the diffused starch chains allowed the formation of a crosslinked network structure (Huang et al., 2017).

Journal Pre-proof

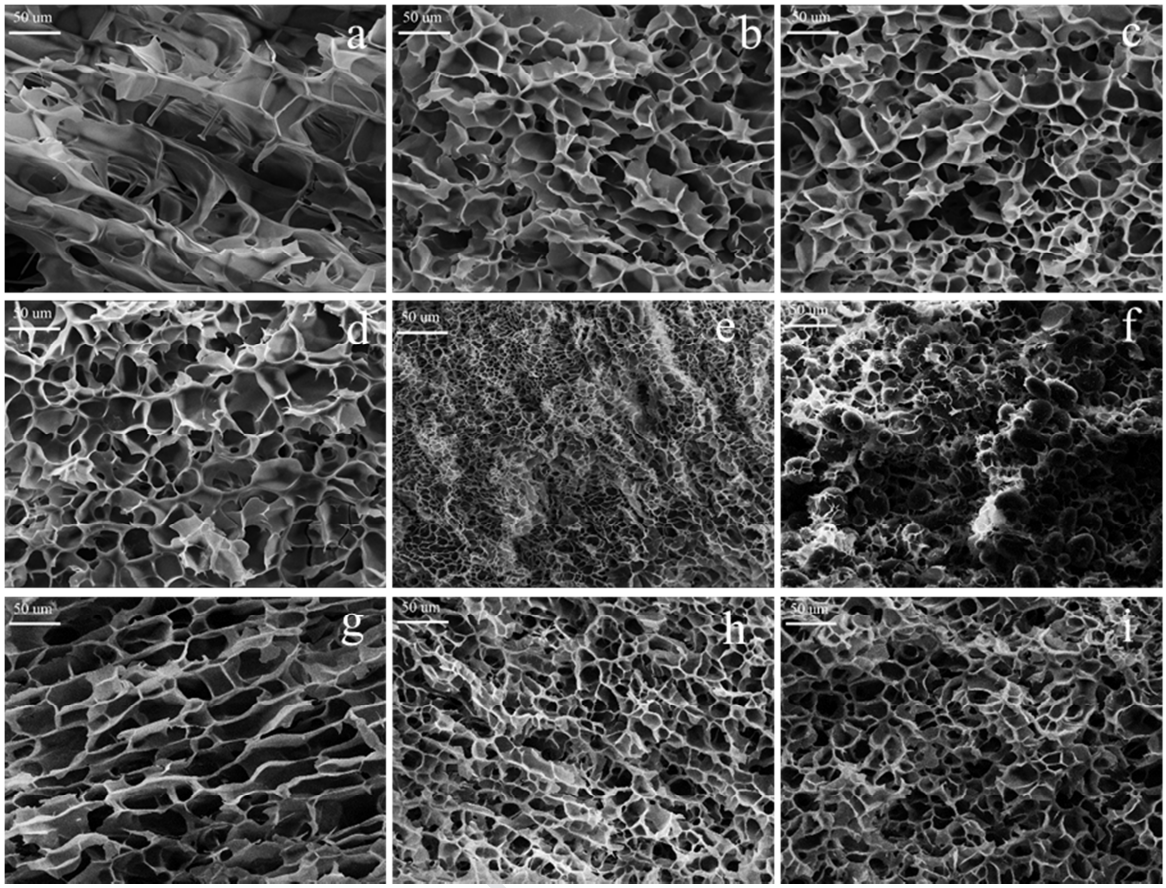

Fig. 1 SEM images of 3D-printed PS samples under different conditions (a, 70 °C/10%; b, 70 °C/15%; c, 70 °C/20%; d, 70 °C/25%; e, 70 °C/30%; f, 60 °C/15%; g, 65 °C/15%; h, 75°C/15%; i, 80 °C/15%).

Under the same printing temperature (70 °C), the PS concentration (10–30%) significantly influenced the morphology of the printed gel. At a low concentration (10%), large cells and thin cell walls could be observed (Fig. 1a). With increasing PS concentration, the cells became smaller and the cell wall became thicker (Fig. 1b-e). A higher cell density can give starch gels higher mechanical strength (Guo et al., 2016).

At the same PS concentration (15%), the printing temperature also significantly affect the morphology of the printed gel. At a printing temperature of 60 °C, there were still some intact PS

Journal Pre-proof

granules embedded in the gelatinized matrix (Fig. 1f). In this case, because of the insufficient gelatinization, there could be limited starch chains diffused out to form a network structure by ways of chain entanglement and hydrogen bonding. Nonetheless, when the printing temperature was higher than 65 °C, starch granule remnants could hardly be found. A higher printing temperature up to 75 °C led to a higher cell density and a smaller cell size (Fig. 1g-h). However, when the temperature was even higher (80 °C), less uniform dispersion of cells could be noticed (Fig. 1i), which might be attributed to the instability of the flow and less effective chain interactions.

The morphological results here show that only at appropriate starch concentration and printing temperature can a PS gel network with uniformly distributed cells be formed, giving acceptable 3D-printability (Liu et al., 2018a).

3.2 Crystalline structure

Fig. 2 shows the XRD patterns of PS samples under different HE-3DP conditions. Native PS displays a B-type crystalline pattern with peaks at 5.6°, 17°, 22.0° and 24.0° 2θ (Xia, Gou, Zhang, Li, & Jiang, 2018; Zhang et al., 2019a). It can be seen in Fig.2a that the diffraction peaks of the PS samples of 10–30% concentration almost disappeared, suggesting the HE-3DP process had mostly destroyed the original crystalline structure. As shown in Fig. 2b, the PS sample printed at 60 °C still exhibited weak B-type diffraction as the original crystallites are partially retained. With higher printing temperatures, the diffraction peak intensity decreased and then disappeared. Given this, the printing temperature controls the crystallinity of the printed PS samples and a high enough temperature could completely gelatinize starch during HE-3DP.

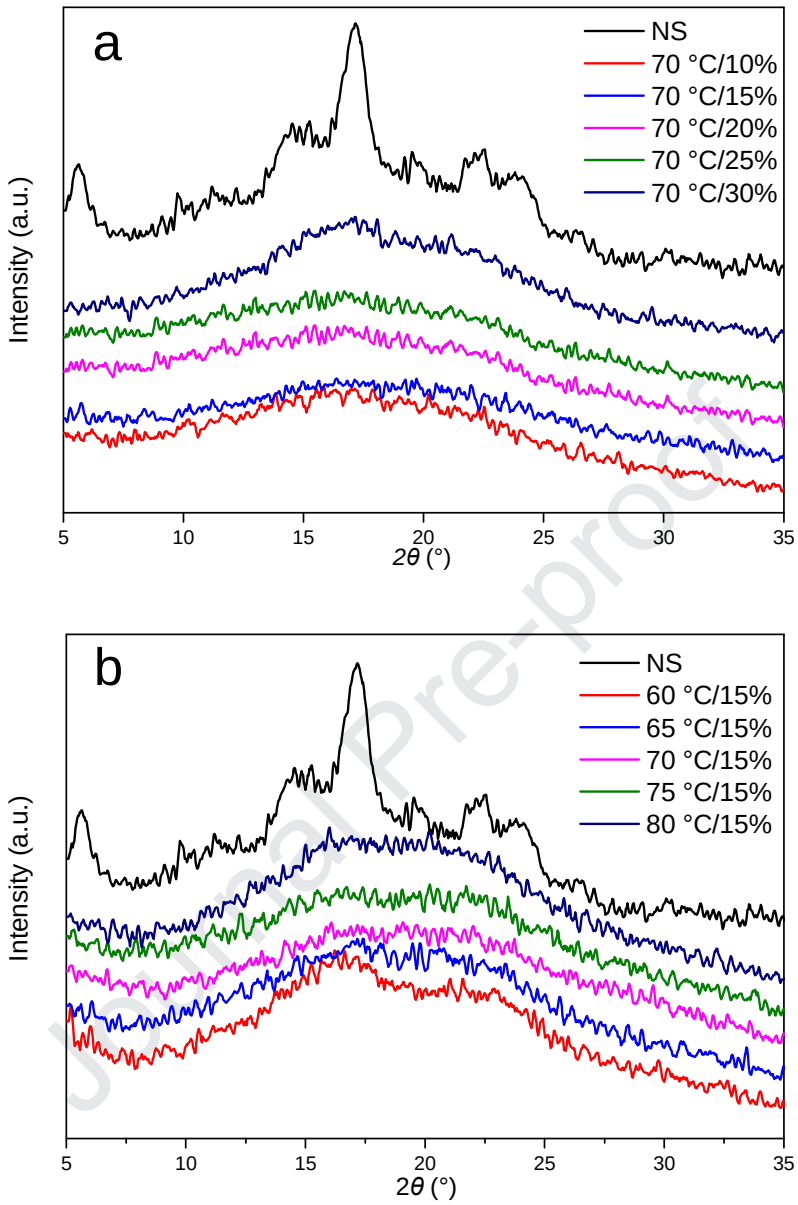

Fig. 2 X-ray diffraction patterns of 3D-printed PS samples under different conditions (a, different concentrations; b, different printing temperatures).

3.3 Short-range ordered structure

The IR absorbance bands at 1045 and 1022 cm^{-1} is associated with the ordered and amorphous structures of starch, respectively. Hence, the ratio of intensity at 1045/1022 cm^{-1}

($R_{1045/1022}$) can be used to measure short-range order (Zhang, Li, Liu, Xie, & Chen, 2013; Liu et al., 2019) (Table 1). Compared with the $R_{1045/1022}$ value of native PS, those values of 3D-printed PS samples were much lower, suggesting the destruction of short-range order. There was no significant difference between the 3D-printed PS samples of different concentrations (10–30%). On the other hand, at a fixed PS concertation of 15%, increasing the printing temperature from 60 °C to 65 °C led to a decrease in short-range order; then increasing the temperature up to 80 °C did not cause further change in short-range order. Therefore, the short-range order of the 3D-printed PS sample was mainly influenced by printing temperature.

Table 1. $R_{1045/1022}$ of printed PS samples under different HE-3DP conditions.[A]

Sample	$R_{1045/1022}$	Sample	$R_{1045/1022}$
NS	0.805±0.002[a]	NS	0.805±0.002[a]
70 °C/10%	0.515±0.004[b]	60 °C/15%	0.601±0.010[b]
70 °C/15%	0.522±0.001[b]	65 °C/15%	0.540±0.004[c]
70 °C/20%	0.525±0.001[b]	70 °C/15%	0.522±0.004[c]
70 °C/25%	0.526±0.007[b]	75 °C/15%	0.529±0.010[c]
70 °C/30%	0.527±0.004[b]	80 °C/15%	0.527±0.014[c]

[A] Values are means ± SD of triplicate tests (n = 3); values followed by the different letter are significantly different ($p < 0.05$).

3.4 Nano-aggregated structure

Due to the difference in the electron density in the starch structure, SAXS can be used to analyze the periodic nanoscale structure, nanoparticle diameter, mesoscopic pore size, shape and

distribution (Chi et al., 2017). To obtain insight into the submicroscopic structure of 3D-printed PS samples, the SAXS curves (Fig. 3a and 3c) were transformed into the Kratky plots (q^2*$I(q)$ *vs.* q) (Fig. 3b and 3d) according to the Lorentz equation. A peak at finite q range over the Kratky plot indicates the presence of a heterogeneous aggregated structure in the gel system (Chi, Li, Zhang, Chen, & Li, 2018). As presented in Fig. 3b, there was no obvious peak in the low q region of 3D-printed PS samples of 10–30% concentration, suggesting a uniform gel structure of the printed samples. This confirms that the crystalline and ordered structure of PS were destroyed by HE-3DP, facilitating the formation of a relatively uniform network structure. As shown in Fig. 3d, a characteristic peak was still observable at about 0.7 nm^{-1} at 60 °C, indicating this temperature was not sufficient to destroy all the original lamellar structure of PS. Printing temperatures higher than that led to the disappearance of the characteristic peak at 0.7 nm^{-1}, indicating HE-3DP at 65–80 °C was enough to destroy the original lamellar structure of PS to form a uniform and stable gel.

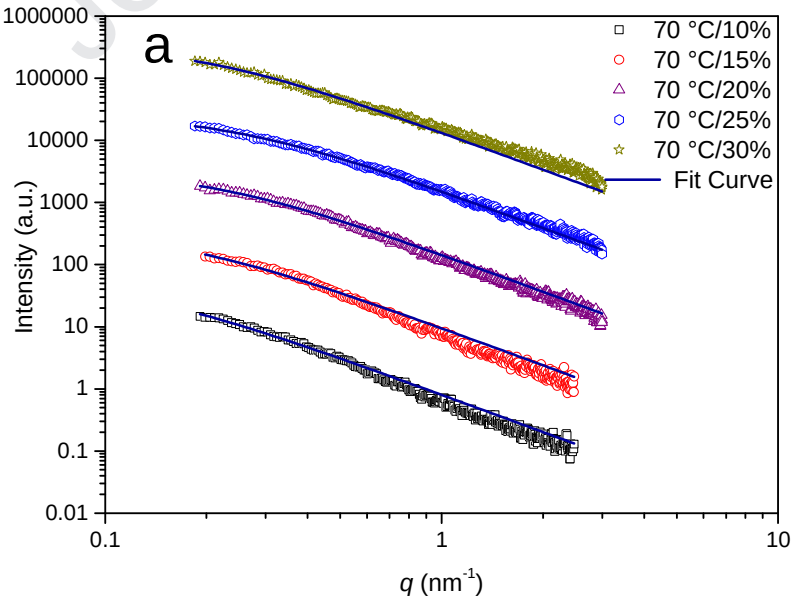

a

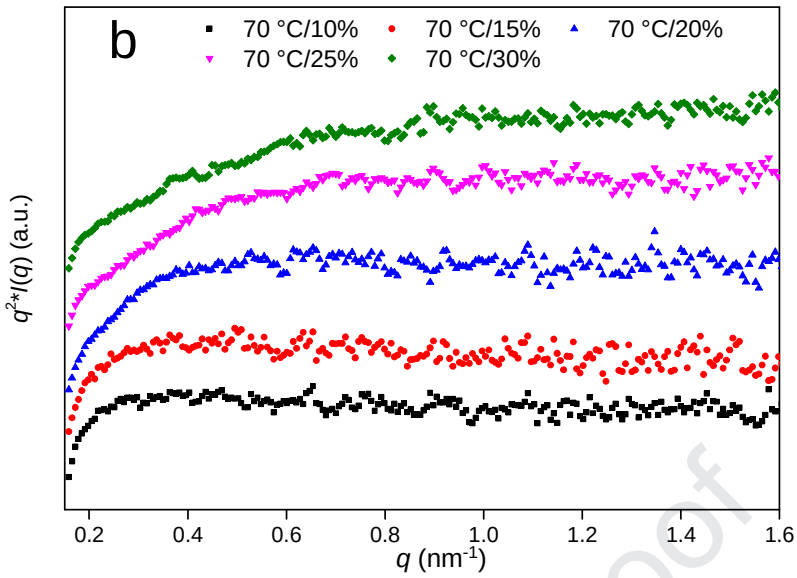

225

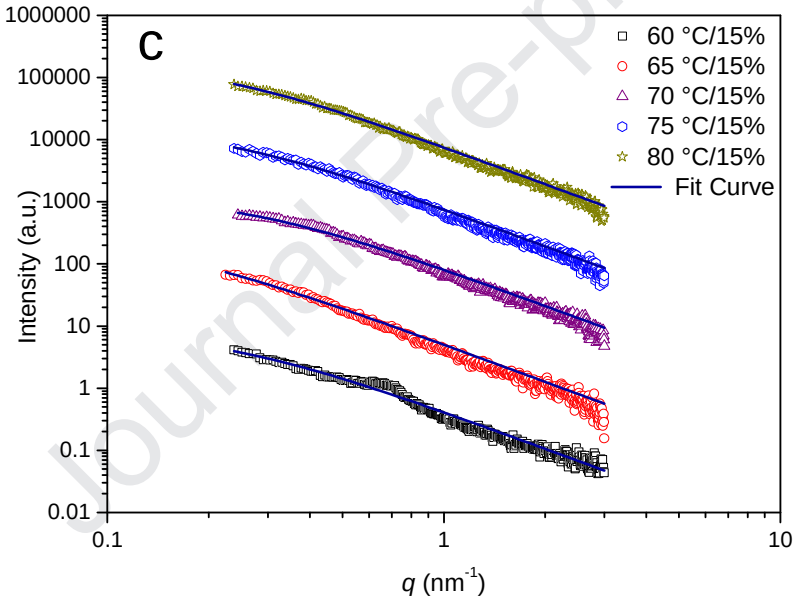

226

Journal Pre-proof

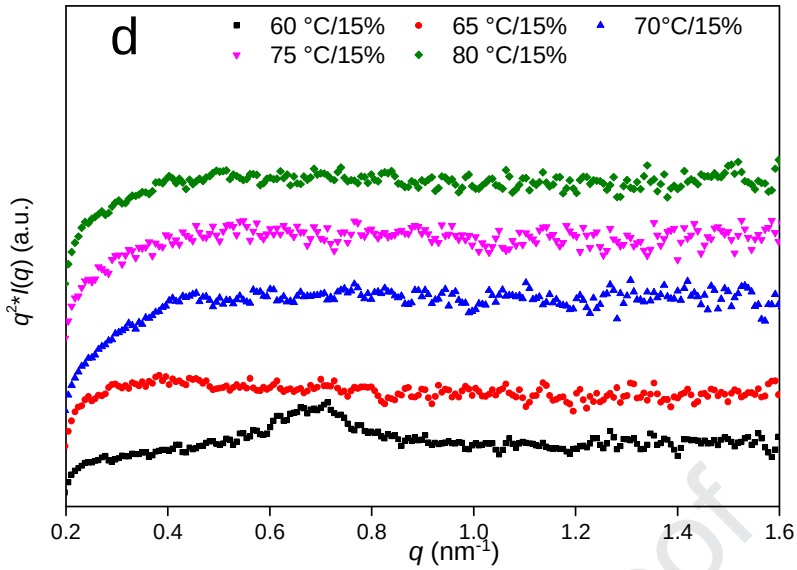

227

228 Fig. 3 SAXS patterns (a and c) and Kratky plots (b and d) of 3D-printed PS samples under different

229 HE-3DP conditions.

230

231 According to previous studies (Emmerling et al., 1995; Hammouda et al., 2004), the SAXS

232 curve of the homogeneous network structure of PS gel was fitted according to the OZ equation (Eq.

233 1) to obtain the correlation length (ξ) to reflect the pore size formed by chain entanglement (note

234 "pores" are different from the "cells" observed in SEM images and are on a much smaller length

235 scale). A greater degree of entanglement in a gel means a lower pore size and lower ξ (Shibayama,

236 2011). The fitting data were shown in Table 2. Almost all the regression coefficients (R^2) for PS

237 samples were higher than 0.99, suggesting the applicability of the OZ equation in this case. This

238 also indicates that 3D-printed PS samples had a uniform structure with little difference in electron

239 density. Increasing the PS concentration from 10 to 30% led to a decrease in ξ, suggesting a denser

240 gel network with smaller pore sizes resulting from a greater degree of chain entanglement (Guo et

241 al., 2016). On the other hand, at a fixed PS concentration of 15%, with the printing temperature

increasing from 65 °C to 80 °C, ξ first increased and then decreased. Regarding this, a higher temperature (up to 70 °C) could be instrumental to gelatinization, but the temperature had to be even higher to allow more free starch chains available for the formation of a homogeneous gel network.

Table 2 Fitting parameters of the SAXS curves of 3D-printed PS samples under different HE-3DP conditions.

Sample	ξ (nm)	R^2	Sample	ξ (nm)	R^2
70 °C/10%	8.43±0.20[a]	0.995	60 °C/15%[A]	–	–
70 °C/15%	6.06±0.11[b]	0.993	65 °C/15%	5.24±0.18[b]	0.993
70 °C/20%	4.79±0.04[c]	0.996	70 °C/15%	6.06±0.11[a]	0.993
70 °C/25%	4.12±0.02[d]	0.998	75 °C/15%	4.86±0.06[c]	0.994
70 °C/30%	2.84±0.01[e]	0.998	80 °C/15%	4.61±0.05[c]	0.997

[A] The sample was a heterogeneous system, for which the OZ equation is not suitable; values followed by the different letter are significantly different ($p < 0.05$)

3.5 Rheological properties

As a viscoelastic material, the starch gel may experience strain under certain stress. When the strain is in the linear viscoelastic region (LVR), the gel structure deforms reversibly but becomes irreversible once the strain exceeds the LVR (Carmona, Ramírez, Calero, & Muñoz, 2014). G' and τ_y reflect the structural strength of the gel, and τ_f represents the required minimum stress for the material to flow, which reflects the difficulty of extrusion (Chen et al., 2019). As shown in Fig 4a-b, G', τ_y, and τ_f had a strong dependence on PS concentration (from 10 to 30%), with G' increasing

Journal Pre-proof

from 282.75 Pa to 1766.82 Pa, τ_y increasing from 44.41 Pa to 883.19 Pa, and τ_f increasing from 192.60 Pa to 2079.45 Pa, at a fixed printing temperature of 70 °C. Regarding this, a higher PS concentration means more starch chains existing within a certain space, which promote chain entanglement leading to a denser network structure with smaller cell sizes and thicker cell walls. In this way, the strength of PS gel was enhanced, although the difficulty of extrusion was also increased due to increased viscosity. As shown in Fig 4c-d, with increasing printing temperature from 60 °C to 80 °C at a fixed PS concentration of 15%, G', τ_y and τ_f showed a trend of first increasing then decreasing. Again, a higher temperature was needed for starch to gelatinize (with granule, crystallites and short-range order being destroyed) so that a homogenous network structure could be formed. A higher temperature was helpful for the release of free starch chains and chain interactions so that a gel with a denser network structure could be formed with higher mechanical strength. However, when the printing temperature was above or equal to 75 °C, the high mobility of starch chains could make the chain interactions less effective and cells less uniform (see SEM images), causing weakened strength. Nonetheless, in this case, τ_f was also reduced indicating better flowability.

Journal Pre-proof

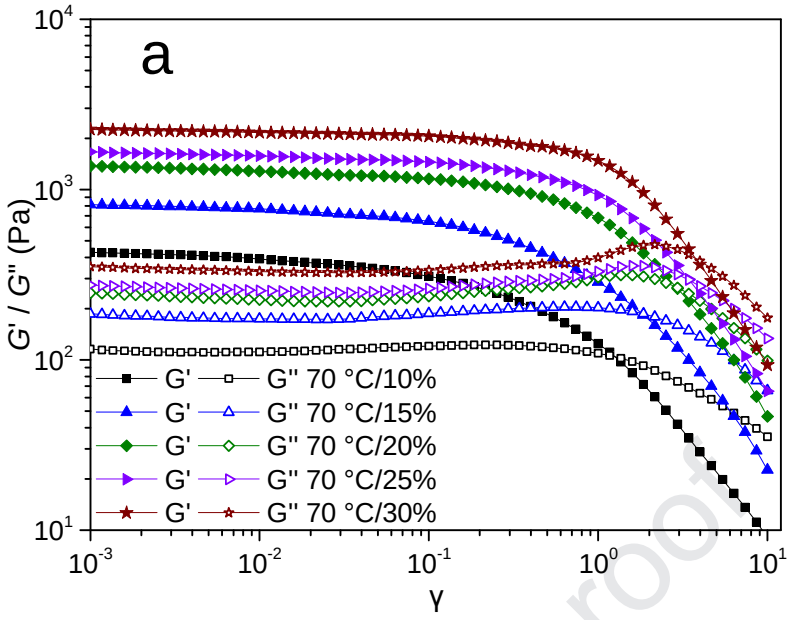

275

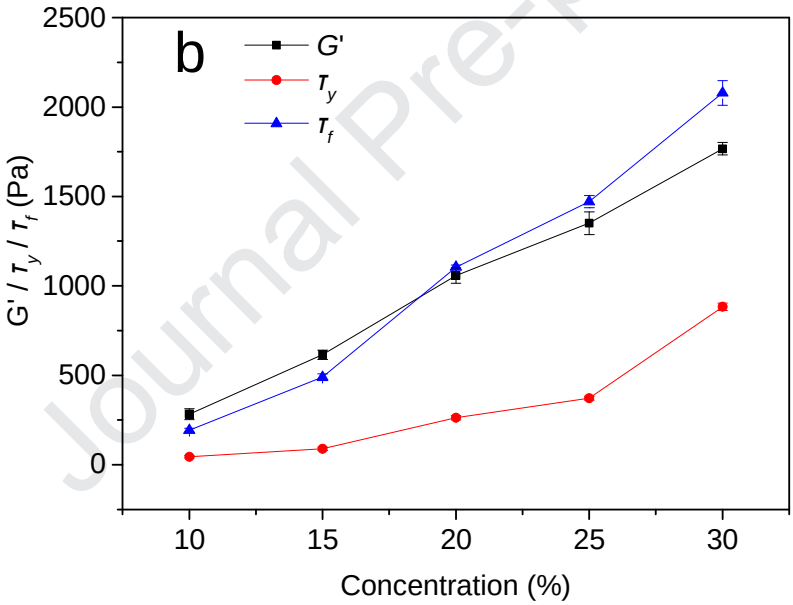

276

Journal Pre-proof

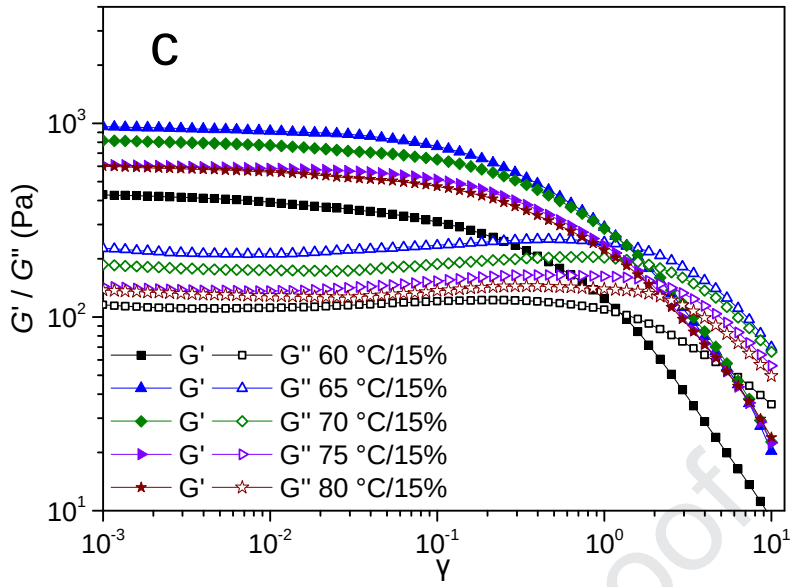

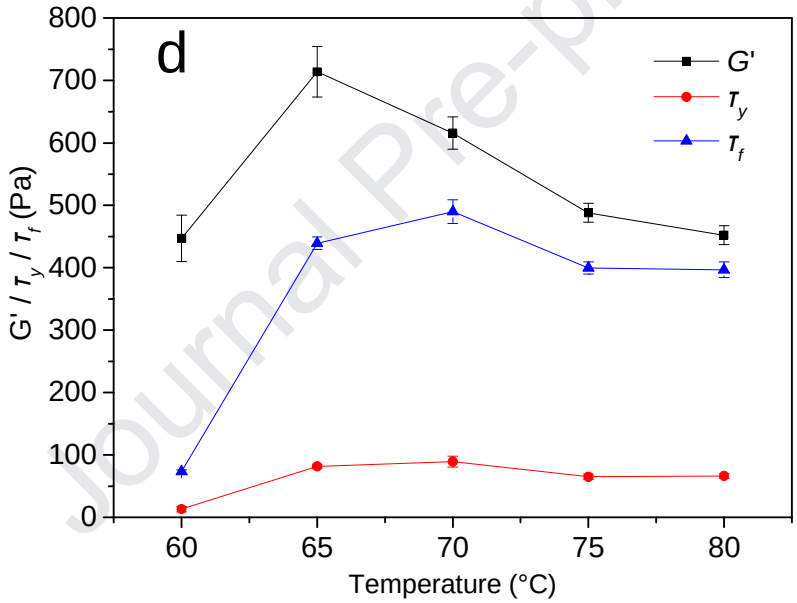

Fig. 4 Strain sweep tests of 3D-printed PS samples under different HE-3DP conditions: a) strain sweep under different concentrations; b) G', τ_y and τ_f under different concentrations; c) strain sweep under different printing temperatures; d) G', τ_y and τ_f under different printing temperatures.

3.6 Printability

Fig. 5a shows the model (50×50×16 mm) used for HE-3DP, for which the PS objects were

constructed by layer-by-layer deposition according to our established procedure (Liu et al., 2018c) under different HE-3DP conditions. The line width and layer number (Table 3) indicate the printing accuracy and structural strength, respectively (Liu et al., 2018b; Chen et al., 2019). From Fig. 5b-d and Table 3, we can see that only the samples at 15% or 20% PS concentration showed good printability. For the PS sample of 10% concentration, there were not enough starch chains in the confined system for chain entanglement and hydrogen-bonding interactions, and the gel network was too weak (low G' and τ_y) to support the subsequently deposited layers, resulting in a wide line width (1.20 mm) and a small layer number (8), with deformation or collapse. A higher PS concentration could lead to a denser gel network with smaller cell sizes and thicker cell walls, as reflected by higher G' and τ_y, which ensure the printing accuracy and strength. Nonetheless, higher τ_f means rising difficulty in extrusion. When the PS concentration was equal or greater than 25%, τ_f became high enough to block the nozzle leading to a failure in printing.

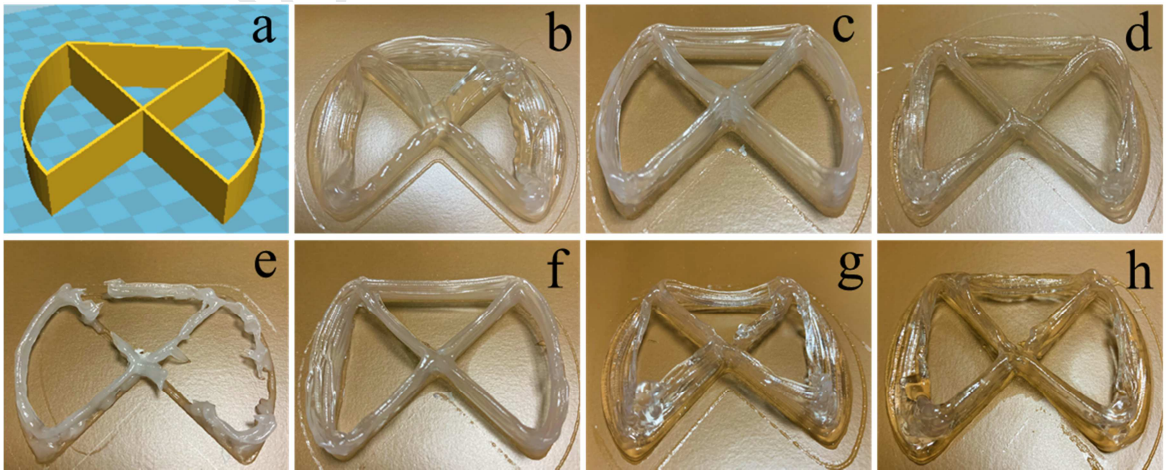

Fig. 5 Printed PS objects under different HE-3DP conditions (a, model (50*50*16 mm); b, 70 °C/10%; c, 70 °C/15%; d, 70 °C/20%; e, 60 °C/15%; f, 65 °C/15%; g, 75 °C/15%; h, 80 °C/15%).

303 Table 3. Line widths and layer numbers of 3D-printed PS objects under different HE-3DP
304 conditions.

Sample	Line width (mm)	Layer numbers	Sample	Line width (mm)	Layer number
70 °C/10%	1.20±0.003[a]	8±0[b]	60 °C/15%	1.14±0.08[a]	5±1[d]
70 °C/15%	0.94±0.006[b]	17±1[a]	65 °C/15%	1.01±0.02[b]	15±0[b]
70 °C/20%	0.92±0.003[c]	17±2[a]	70 °C/15%	0.94±0.01[d]	17±0[a]
70 °C/25%	PF[A]	PF	75 °C/15%	0.95±0.02[cd]	12±1[c]
70 °C/30%	PF	PF	80 °C/15%	0.98±0.08[c]	11±1[c]

305 [A] PF means printing failed; values are means ± SD of triplicate tests (n = 3); values followed by the different
306 letter are significantly different ($p < 0.05$).

307

308 Fig. 5e-f and Table 3 show that printing temperature, as a key factor affecting the rheological
309 properties of PS samples, had a significant effect on the printability. The printed object at 60 °C
310 was milky white and discontinuous with low printability. In this case, PS was not fully gelatinized
311 with part of the original crystalline and lamellar structures retained. Thus, there were not enough
312 free starch chains in the system to undergo chain entanglement and hydrogen bonding, resulting in
313 an uneven gel network with low G' and τ_y, and thus low printing accuracy and poor strength. With
314 increasing printing temperature, sufficient chain interactions led to a homogeneous gel network
315 with increased G' and τ_y and, thus, high printability. In this way, the accuracy and layer number of
316 the PS object increased. In particular, a printing temperature of 70 °C and a PS concentration of 15%
317 could result in excellent line width (0.94 mm) and layer number (17). However, when the printing
318 temperature was even higher (≥75 °C), the interactions between starch chains became less effective,
319 causing a decrease in strength with lower G' and τ_y and thus lower printability.

320

3.7 Correlation

Table 4 shows Pearson correlation coefficients calculated for the relationship among the structure, rheological properties and printability of PS samples under different HE-3DP conditions. It can be seen that ξ had a significant positive correlation between line width. Regarding this, lower ξ can be linked to the less swelling of the printed sample, leading to better printing accuracy. However, the correction between ξ and rheological properties was not evident. In this regard, it is necessary to find other indicators to more accurately reflect the network gel structure. In addition, $R_{1045/1022}$ was not seen to be significantly correlated with G', τ_y, τ_f, line width, and line number. This means the short-range ordered structure was not key in determining the rheological properties and printability in the temperature range of 70–80 °C.

There was a significant positive correlation among the rheological parameters (G', τ_y and τ_f), which is in agreement with the curves shown in Fig. 4b and d. All these rheological parameters were strongly influenced by PS concentration which affected the gel density and by printing temperature which determined the mobility of starch chains. Moreover, the rheological properties had a positive correlation with layer number but a negative correlation with line width. In this regard, with sufficient G' and τ_y, the next printed layer could be supported without deformation or collapse.

Table 4. Pearson correlation coefficients for the relationship among the structure, rheological properties and printability of PS samples.[A]

	$R_{1045/1022}$	ξ	G'	τ_y	τ_f	Line width	Layer number
$R_{1045/1022}$	1						

ξ	-0.675	1					
G'	-0.406	-0.214	1				
τ_y	-0.204	-0.117	0.856*	1			
τ_f	-0.151	-0.224	0.862*	0.989**	1		
Line width	-0.448	0.880*	-0.499	-0.305	-0.378	1	
Layer number	0.383	-0.522	0.500	0.524	0.547	-0.779	1

[A] Values followed by * have a significant correlation ($p < 0.05$).

4 Conclusion

This study shows the importance of controlling the PS concentration and printing temperature for controlling the printability of PS for HE-3DP. A high enough PS concentration was necessary for the formation of a gel structure with suitable rheological properties for printing. However, when the PS concentration was too high (25%), τ_f of the PS sample became too high to block the nozzle leading to a failure in printing. On the other hand, the printing temperature had to be high enough to ensure full gelatinization and the release of starch chains for the gel formation. Nevertheless, when the printing temperature was equal to or above 75 °C, the interactions between starch chains may become less effective, resulting in weakened mechanical strength and poor printability of the PS-based ink. Moreover, appropriate G', τ_y and τ_f of the PS material are the key to ensure the printability in HE-3DP. In all, this work provides important information for the design of personalized high-quality starch-based food by HE-3DP.

Acknowledgements

This research has been financially supported by the National Natural Science Foundation of

China (NSFC)-Guangdong Joint Foundation Key Project (U1501214), the Key Project of Guangzhou Science and Technology program (No.201804020036), and the National Natural Science Foundation of China (31871751). F. Xie acknowledges support from the European Union's Horizon 2020 research and innovation programme under the Marie Skłodowska-Curie grant agreement No. 798225.

Conflict of interests

The authors declare to have no conflict of interests.

References

Ai, Y., & Jane, J.-l. (2015). Gelatinization and rheological properties of starch. *Starch - Stärke*, 67, 213-224.

Carmona, J. A., Ramírez, P., Calero, N., & Muñoz, J. (2014). Large amplitude oscillatory shear of xanthan gum solutions. Effect of sodium chloride (nacl) concentration. *Journal of Food Engineering*, 126, 165-172.

Chen, B., Zhang, B., Li, M.-N., Xie, Y., & Chen, H.-Q. (2018). Effects of glutenin and gliadin modified by protein-glutaminase on pasting, rheological properties and microstructure of potato starch. *Food Chemistry*, 253, 148-155.

Chen, H., Xie, F., Chen, L., & Zheng, B. (2019). Effect of rheological properties of potato, rice and corn starches on their hot-extrusion 3d printing behaviors. *Journal of Food Engineering*, 244, 150-158.

Chi, C., Li, X., Zhang, Y., Chen, L., & Li, L. (2018). Understanding the mechanism of starch digestion mitigation by rice protein and its enzymatic hydrolysates. *Food Hydrocolloids*, 84, 473-480.

Chi, C., Li, X., Zhang, Y., Chen, L., Li, L., & Wang, Z. (2017). Digestibility and supramolecular structural

Journal Pre-proof

changes of maize starch by non-covalent interactions with gallic acid. *Food & function*, 8, 720-730.

Cieśla, K., Sartowska, B., & Królak, E. (2015). Sem studies of the structure of the gels prepared from untreated and radiation modified potato starch. *Radiation Physics and Chemistry*, 106, 289-302.

Dankar, I., Haddarah, A., Omar, F. E. L., Sepulcre, F., & Pujolà, M. (2018). 3d printing technology: The new era for food customization and elaboration. *Trends in Food Science & Technology*, 75, 231-242.

Dankar, I., Pujolà, M., El Omar, F., Sepulcre, F., & Haddarah, A. (2018). Impact of mechanical and microstructural properties of potato puree-food additive complexes on extrusion-based 3d printing. *Food and Bioprocess Technology*, 11, 2021-2031.

Dong, X., Huang, Y., Pan, Y., Wang, K., Prakash, S., & Zhu, B. (2019). Investigation of sweet potato starch as a structural enhancer for three-dimensional printing of scomberomorus niphonius surimi. *Journal of Texture Studies*, 50, 316-324.

Emmerling, A., Petricevic, R., Beck, A., Wang, P., Scheller, H., & Fricke, J. (1995). Relationship between optical transparency and nanostructural features of silica aerogels. *Journal of Non-Crystalline Solids*, 185, 240-248.

Godoi , F. C., Prakash, S., & Bhandari, B. R. (2016). 3d printing technologies applied for food design: Status and prospects. *Journal of Food Engineering*, 179, 44-54.

Guo, L., Hu, J., Zhang, J., & Du, X. (2016). The role of entanglement concentration on the hydrodynamic properties of potato and sweet potato starches. *International Journal of Biological Macromolecules*, 93, 1-8.

Hammouda, B., Ho, D. L., & Kline, S. (2004). Insight into clustering in poly(ethylene oxide) solutions. *Macromolecules*, 37, 6932-6937.

Han, H., Hou, J., Yang, N., Zhang, Y., Chen, H., Zhang, Z., Shen, Y., Huang, S., & Guo, S. (2019). Insight on the changes of cassava and potato starch granules during gelatinization. *International Journal of Biological Macromolecules*, 126, 37-43.

Huang, J., Wei, M., Ren, R., Li, H., Liu, S., & Yang, D. (2017). Morphological changes of blocklets during the gelatinization process of tapioca starch. *Carbohydrate Polymers*, 163, 324-329.

Ibanoğlu , Ş., Özaslan, Z. T., & Ibanoğlu, E. (2018). Effects of ultrasonication and aqueous ozonation on gelatinization and flow properties of potato starch. *Ozone: Science & Engineering*, 40, 105-112.

Juszczak, L., Witczak, M., Ziêba, T., & Fortuna, T. (2012). Rheological behaviour of heated potato starch dispersions. *International Agrophysics*, 26, 381-386.

Krystyjan, M., Ciesielski, W., Khachatryan, G., Sikora, M., & Tomasik, P. (2015). Structure, rheological, textural and thermal properties of potato starch – inulin gels. *LWT - Food Science and Technology*, 60, 131-136.

Le Tohic, C., O'Sullivan, J. J., Drapala, K. P., Chartrin, V., Chan, T., Morrison, A. P., Kerry, J. P., & Kelly, A. L. (2018). Effect of 3d printing on the structure and textural properties of processed cheese. *Journal of Food Engineering*, 220, 56-64.

Lille, M., Nurmela, A., Nordlund, E., Metsä-Kortelainen, S., & Sozer, N. (2018). Applicability of protein and fiber-rich food materials in extrusion-based 3d printing. *Journal of Food Engineering*, 220, 20-27.

Liu, Y., Chen, L., Xu, H., Liang, Y., & Zheng, B. (2019). Understanding the digestibility of rice starch-gallic acid complexes formed by high pressure homogenization. *International Journal of Biological Macromolecules*, 134, 856-863.

Journal Pre-proof

Liu, Z., Bhandari, B., Prakash, S., & Zhang, M. (2018a). Creation of internal structure of mashed potato construct by 3d printing and its textural properties. *Food Research International*, 111, 534-543.

Liu, Z., Zhang, M., Bhandari, B., & Wang, Y. (2017). 3d printing: Printing precision and application in food sector. *Trends in Food Science & Technology*, 69, 83-94.

Liu, Z., Zhang, M., Bhandari, B., & Yang, C. (2018b). Impact of rheological properties of mashed potatoes on 3d printing. *Journal of Food Engineering*, 220, 76-82.

Liu, Z., Zhang, M., & Yang, C.-h. (2018c). Dual extrusion 3d printing of mashed potatoes/strawberry juice gel. *LWT*, 96, 589-596.

Martínez-Monzó, J., Cárdenas, J., & García-Segovia, P. (2019). Effect of temperature on 3d printing of commercial potato puree. *Food Biophysics*, 14, 225-234.

Mirarab Razi, S., Motamedzadegan, A., Shahidi, A., & Rashidinejad, A. (2018). The effect of basil seed gum (bsg) on the rheological and physicochemical properties of heat-induced egg albumin gels. *Food Hydrocolloids*, 82, 268-277.

Przetaczek-Rożnowska, I. (2017). Physicochemical properties of starches isolated from pumpkin compared with potato and corn starches. *International Journal of Biological Macromolecules*, 101, 536-542.

Shibayama, M. (2011). Small-angle neutron scattering on polymer gels: Phase behavior, inhomogeneities and deformation mechanisms. *Polymer Journal*, 43, 18-34.

Sun, J., Zhou, W., Huang, D., Fuh, J. Y. H., & Hong, G. S. (2015). An overview of 3d printing technologies for food fabrication. *Food and Bioprocess Technology*, 8, 1605-1615.

Sun, J., Zhou, W., Yan, L., Huang, D., & Lin, L.-y. (2018). Extrusion-based food printing for digitalized food design and nutrition control. *Journal of Food Engineering*, 220, 1-11.

Journal Pre-proof

Xia, T., Gou, M., Zhang, G., Li, W., & Jiang, H. (2018). Physical and structural properties of potato starch modified by dielectric treatment with different moisture content. *International Journal of Biological Macromolecules*, 118, 1455-1462.

Yang, F., Zhang, M., Bhandari, B., & Liu, Y. (2018). Investigation on lemon juice gel as food material for 3d printing and optimization of printing parameters. *LWT - Food Science and Technology*, 87, 67-76.

Yang, F., Zhang, M., Fang, Z., & Liu, Y. (2019). Impact of processing parameters and post-treatment on the shape accuracy of 3d-printed baking dough. *International Journal of Food Science & Technology*, 54, 68-74.

Zhang, B., Li, X., Liu, J., Xie, F., & Chen, L. (2013). Supramolecular structure of a- and b-type granules of wheat starch. *Food Hydrocolloids*, 31, 68-73.

Zhang, B., Zhou, W., Qiao, D., Zhang, P., Zhao, S., Zhang, L., & Xie, F. (2019a). Changes in nanoscale chain assembly in sweet potato starch lamellae by downregulation of biosynthesis enzymes. *Journal of Agricultural and Food Chemistry*, 67, 6302-6312.

Zhang, Y.-F., Li, J.-B., Zhang, Z.-Y., Wei, Q.-S., & Fang, K. (2019b). Rheological law of change and conformation of potato starch paste in an ultrasound field. *Journal of Food Measurement and Characterization*, 13, 1695–1704.

Zheng, L., Yu, Y., Tong, Z., Zou, Q., Han, S., & Jiang, H. (2019). The characteristics of starch gels molded by 3d printing. *Journal of Food Processing and Preservation*, 43, 1-11.

Journal Pre-proof

Journal Pre-proof

Highlights

- ✓ Concentration and temperature controls the 3D printability of potato starch (PS)
- ✓ Suitable PS concentration facilitates chain interactions
- ✓ Adequate temperature ensures a homogenous network structure.
- ✓ G', τ_y and τ_f are associated with PS concentration and printing temperature
- ✓ Structure, rheological properties and printability of PS materials are correlated.

Journal Pre-proof

Journal Pre-proof

– Declaration of Interest –

Understanding the structure and rheological properties of potato starch induced by hot-extrusion 3D printing

Zipeng Liu [a], Huan Chen [a], Bo Zheng [a], Fengwei Xie [b,c,], Ling Chen [a,*]**

[a] *Ministry of Education Engineering Research Center of Starch & Protein Processing, Guangdong Province Key Laboratory for Green Processing of Natural Products and Product Safety, School of Food Science and Engineering, South China University of Technology, Guangzhou 510640, China*

[b] *International Institute for Nanocomposites Manufacturing (IINM), WMG, University of Warwick, Coventry CV4 7AL, United Kingdom*

[c] *School of Chemical Engineering, The University of Queensland, Brisbane, Qld 4072, Australia*

The authors declare that there is no conflict of interest regarding the publication of this article.

Journal Pre-proof